MECHANICAL PROPERTIES OF INNOVATIVE MULTIFUNCTIONAL CROSS LAMINATED TIMBER

Authors:
Matthias Arnold[1]; Philipp Dietsch[2]; Stefan Winter[1]

[1]Technical University of Munich
Department of Civil, Geo and Environmental Engineering
Chair of Timber Structures and Building Construction
arnold@tum.de, winter@tum.de

[2]University of Innsbruck
Unit of Timber Engineering
philipp.dietsch@uibk.ac.at

Date 05.04.2021

This article is submitted and accepted for the World Conference on Timber Engineering 2020/21 Santiago, Chile (WCTE 2020/21).

Abstract

This paper deals with wall elements from massive timber, which are modified for thermal activation – multifunctional cross laminated timber (multifunctional CLT). This wood product is currently developed towards maturity for application, by determining e.g. the mechanical properties. The multifunctional CLT elements feature channels in which conditioned air circulates, reducing the cross-sectional area. In this paper we investigate e.g. the compression strength and stiffness, the buckling load, the in-plane shear strength and stiffness and the torsional stiffness properties of multifunctional CLT by means of extensive series of mechanical testing. In addition, the deformation behavior of multifunctional CLT under moisture changes as well as possible cracking in the front layers will be analyzed.

Keywords

massive timber, cross laminated timber, multifunctional cross laminated timber, thermal activation, mechanical properties, compression strength, buckling load, in-plane shear strength, torsional stiffness

1 Introduction

The objective of the research presented is to further develop a previously suggested CLT element (proof-of-concept [1] [2]), multifunctional in terms of its thermal activation, towards maturity for application. CLT wall elements featuring channels in which conditioned air circulates enable the conditioning of massive timber buildings meeting the energy standards currently required in Central Europe.

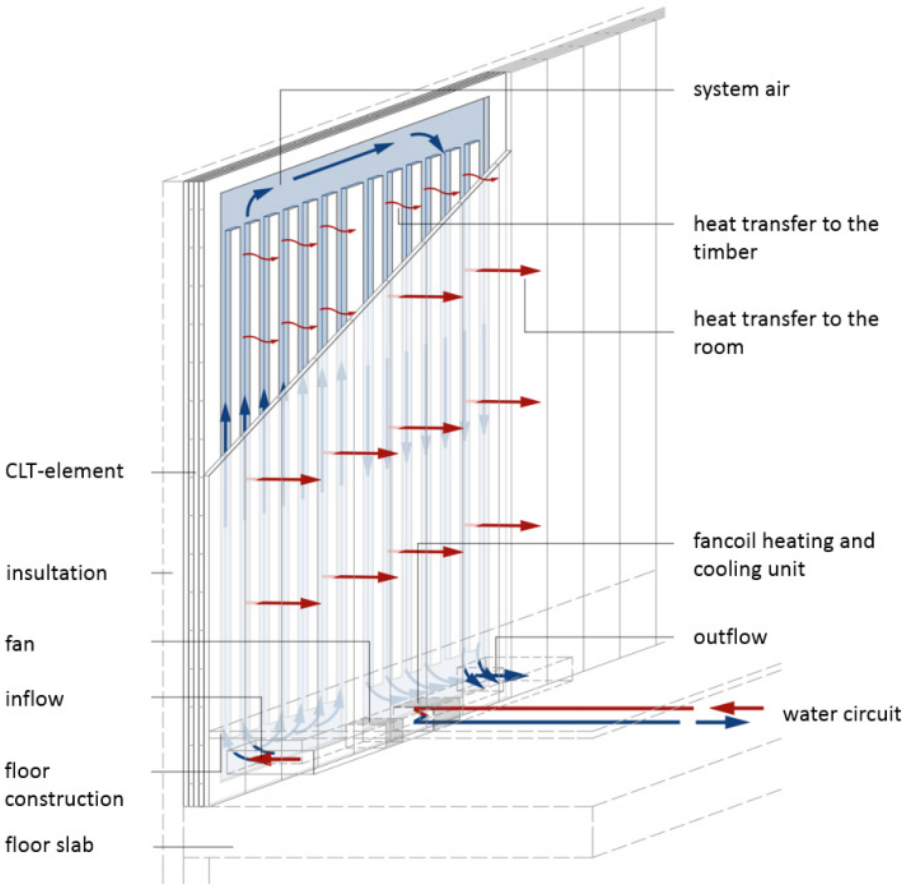

Figure 1: Basic structure of the thermally activated solid timber elements [1]

2 Development and Production of Test Series

2.1 Layups

Towards this aim, multiple series of mechanical and climatic experiments were carried out at Technical University of Munich.

Five different configurations of multifunctional CLT were developed and produced (Series M-1 to M-5). These series feature channels in the functional layer and being covered with an airtight front layer (edge-glued). To enable a quantitative evaluation, the results of the experiments are compared to the results of a reference series on conventional CLT without channels (Series O-1). Table 1 gives an overview of the test series including all necessary dimensions (layers oriented in local x-direction are written bold).

Table 1: Overview of test series and their layup [mm]

Series		M-1	M-2	M-3	M-4	M-5	O-1
Layers		5	5	5	5	6	5
Layup	1	**20**	**20**	**20**	**20**	**20**	**20**
	2	20	20	20	20	20	20
	3	**20**	**20**	**20**	**20**	**20**	**20**
	4	[1)]20	[1)]20	[1)]**20**	20	20	20
	5	[2)]**19**	[3)]**19**	[2)]19	[1)]**20**	[1)]**20**	**20**
	6	/	/	/	/	[3)]**12**	/

[1)] layer with channels; width and distance of the channels $w_{ch} = e_{ch} = 40$ mm

[2)] 1-layered solid wood panel

[3)] 3-layered solid wood panel

2.2 Material Parameters and Gluing

Figure 2 gives the asymmetric cross-sections of the multifunctional CLT series featuring channels in one of its layers. The basic component of each series is a standardized CLT element according to ETA-20/0023 [3]. For M-1 to M-3 series, a 3-layered basic CLT is bonded to the previously manufactured functional layers using a 1-K PUR adhesive, Type I [4] according to DIN EN 301 [5] (red line in Fig. 2). The gluing between the 5th layer (front layer) and 4th layer is also achieved with a 1-K PUR adhesive [6]. The M-4, M-5 and O-1 series consist of a five-layered CLT element in which the channels are milled (except O-1 reference series).

The front layer of the M-1 and M-3 series consist of a single-layered solid wood panel made of silver fir, which is finger-jointed and edge-glued, according to EN 12775 [7]. The front layer

of the M-2 and M-5 series consist of a 3-layerd solid wood panel according to EN 13986 [8] (SWP/3 according to EN 13353 [9]).

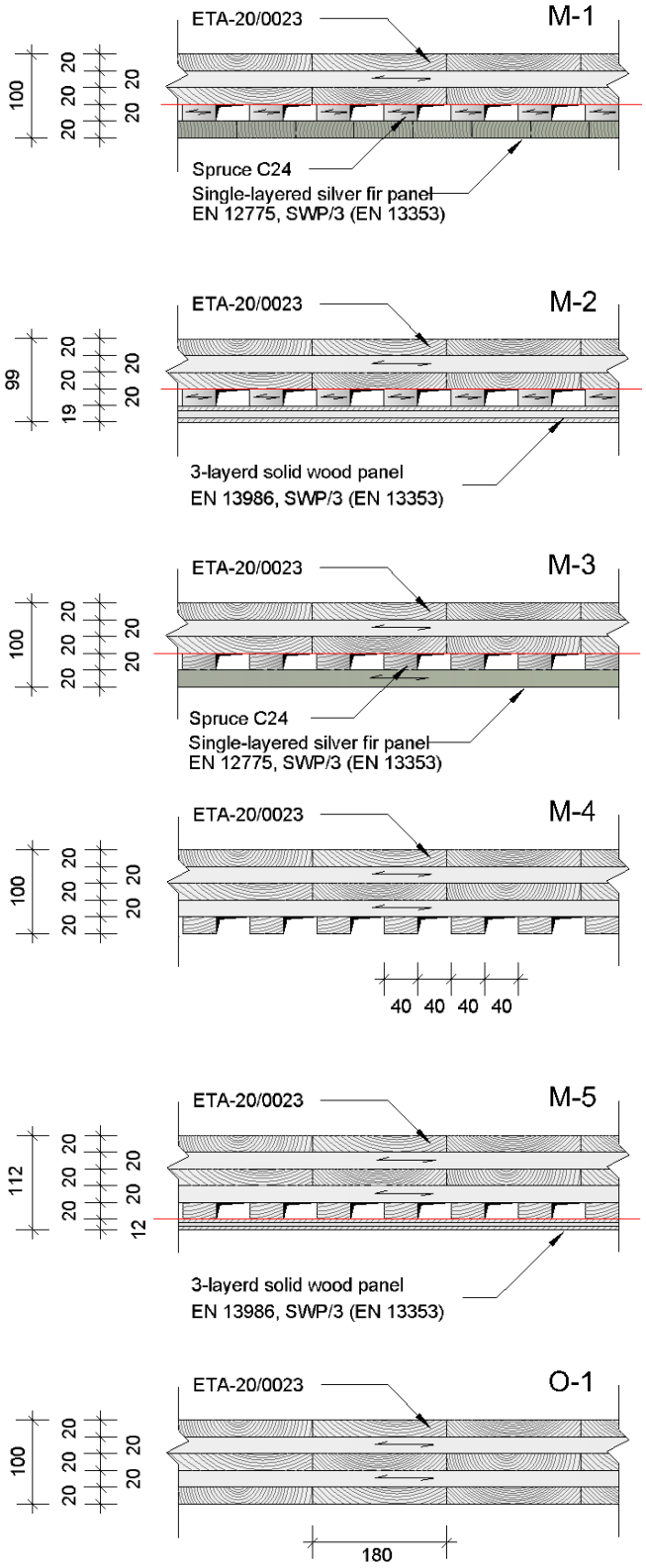

Figure 2: Timber products used for the manufacturing of the series [mm]

3 Mechanical Testing

3.1 Test Programme

The main objective of the mechanical testing is to determine the essential strength and stiffness properties of the multifunctional CLT. Table 2 lists the mechanical experiments carried out on the multifunctional CLT. Hereby we will show, that the front layer as well as the layers including the channels are not to be neglected during static dimensioning of multifunctional wall elements.

Table 2: Mechanical investigations

Experiments	processing status
Compression Strength	✓
Buckling Loads	✓
In-plane Shear Stiffness	✓
Torsional Stiffness	✓

The moisture content of each specimens was measured in a depth of 15 mm by means of ram in electrodes after the delivery and was in the range of 12±2% for all series. In addition, kiln drying tests were carried out to determine the density distribution. The homogenized density distribution of the series is given in Figure 3.

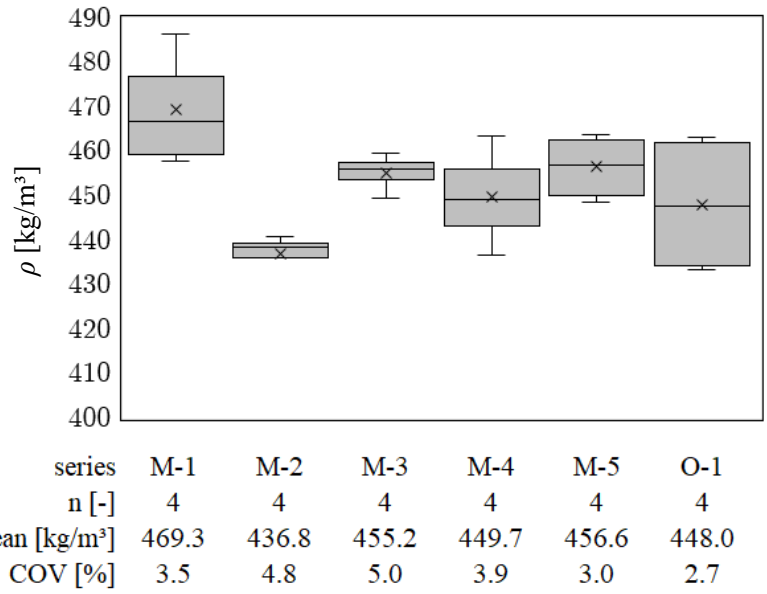

Figure 3: Density distribution of the multifunctional CLT test series (M1-M5) and reference series (O1)

3.2 Compression Strength & Stiffness

3.2.1 Experiments

The modulus of elasticity $E_{c,o}$ (MOE) of each series as well as the compression strength $f_{c,o}$ are determined by compression tests according to EN 408 [10] (Figure 4). Four specimens (*w/h=160mm/400mm)* are taken from each series. The deformation is measured with two displacement transducers, which are attached one on each side of the specimens. The average moisture content of the specimens before the compression tests was u_{mean} = 10.3% (COV 4.8%).

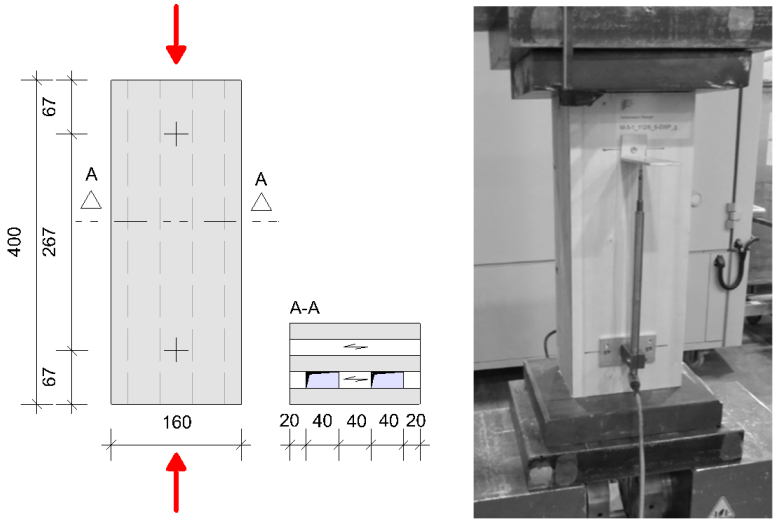

Figure 4: Test setup of the compression tests

3.2.2 Results

The results of the compression tests are given in Figures 5 and 6 (compression strength and modulus of elasticity).

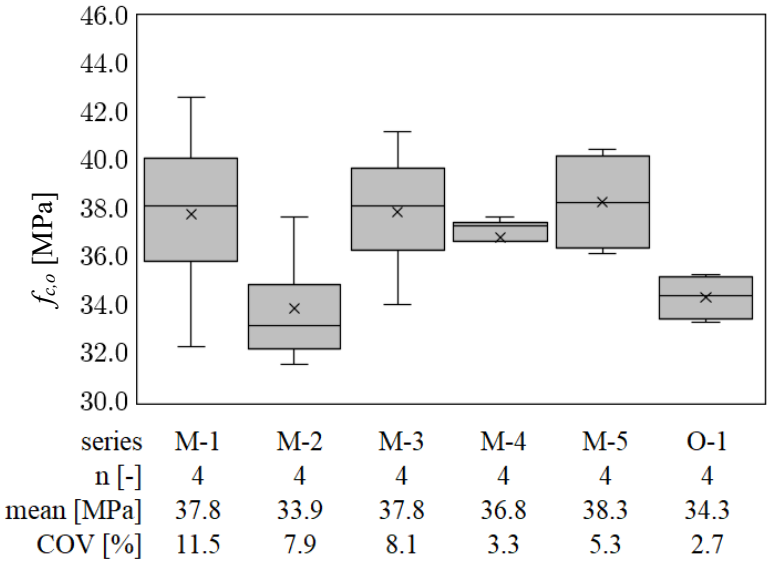

Figure 5: Overall compression strength of multifunctional CLT from different layups

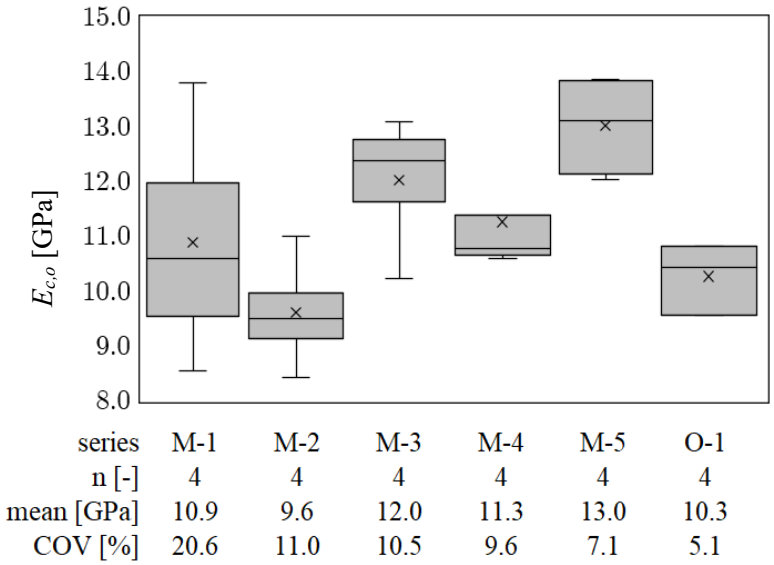

Figure 6: Modulus of elasticity (MOE) determined from the compression tests

When determining the compression strengths and moduli of elasticity, only the cross-sectional components with grain direction parallel to the loading direction are taken into account. For reference series O1 a mean value for the compression strengths $f_{c,0,mean}$ of 34.3 MPa is achieved. The mean value of the modulus of elasticity for reference series O-1 is

10282 MPa (Figure 6). In comparison, according to the European Technical Assessment [3], the value of the MOE is given as 11000 MPa. The maximum value of the MOE is reached by series M-4, including the additional 6th layer made of the 3-layered solid wood panel. The partly higher compression strengths and MOE of series with channels can be explained with the high quality of the front layer (5th layer) partly in combination with the orientation of the functional layer (4th layer).

3.3 Buckling Loads

3.3.1 Experiments

An important parameter for evaluating the load-bearing capacity of multifunctional wall elements is the determination of the buckling loads. For this purpose, four wall elements (w/h=500mm/2950mm) of each series are loaded until collapse (Figure 7). Thereby the external force, the horizontal deflections as well as the strains in the outer lamellas are documented over time.

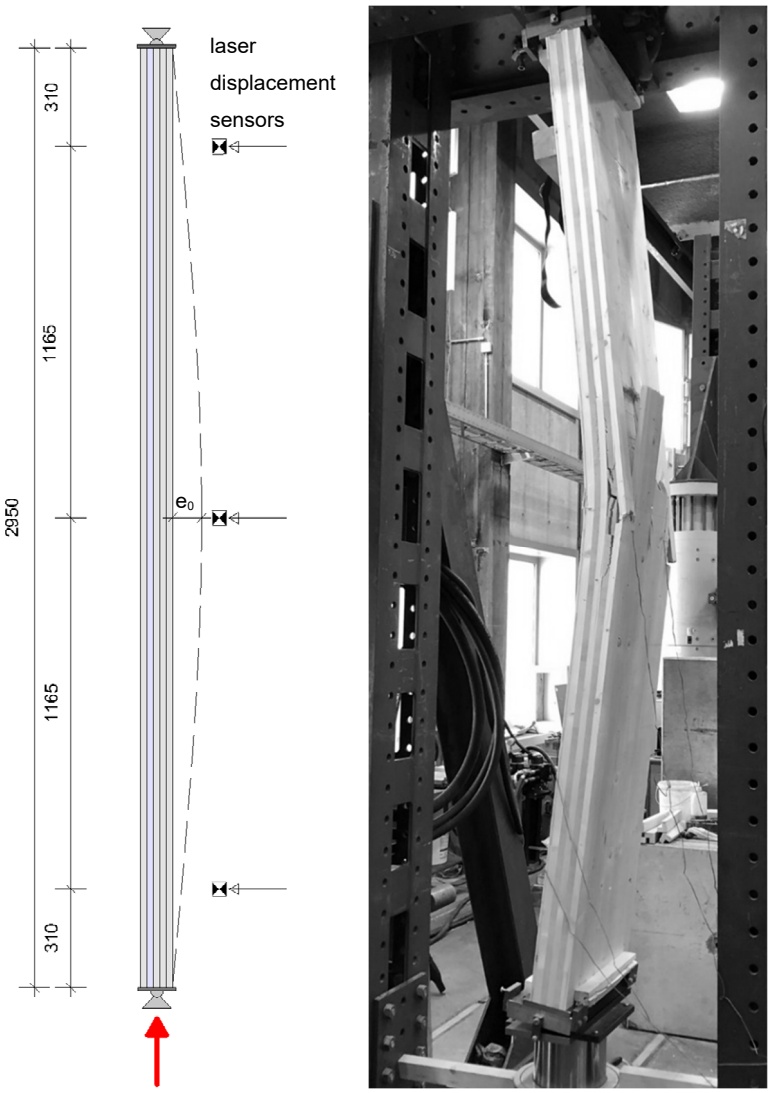

Figure 7: Buckling test on multifunctional CLT wall elements

The testing is carried out force-controlled at a rate of 2 kN/s. The average moisture content of each specimen before testing was u_{mean} = 11.9% (COV 7.9%). The three optical distance sensors not only measure the curvature of the elements over time, but also ensure vertical

positioning of all test specimens as well as the determination of a possible pre-curvature e_0 from production or storage (Table 3). The specimens are loaded in their geometric centre, i.e. without externally applied eccentricity. Only one out of four specimens of the reference series O-1 is tested with an eccentricity of 20 mm each at the wall head and wall foot for the evaluation of later FEM modelling.

3.3.2 Theoretical Investigations

In order to show in the follow-up to the experiments that the calculation of buckling loads of solid wood elements with asymmetric layup and channels is also covered by theoretical calculation methods, the required stiffness and strength parameters are determined for each series (Table 3). The asymmetric layup results in a displacement of the center of gravity of each element and thus an internal eccentricity e_i. This eccentricity is i.a. taken into account when calculating the bending stiffnesses according to the shear analogy method [11] given in [12]. The mean values of the bending strengths are derived from the characteristic strength values of the individual components according to the probabilistic model code of the JCSS [13]. Hence, a logarithmic normal distribution with COV 15% is assumed.

Table 3: Mean values of the strength and stiffness values for the theoretical determination of the buckling loads

Series	[1)] e_0	e_i	[2)] B_x	[3)] f_m	[4)] $f_{c,o}$	[4)] $E_{c,o}$
	[mm]	[mm]	[MNm²/m]	[MPa]	[MPa]	[MPa]
M-1	1.79	7.00	0.731	30.7	37.8	10.9
M-2	2.99	7.07	0.671	31.5	33.9	9.6
M-3	1.77	7.00	0.378	30.7	37.9	12.0
M-4	-0.27	9.00	0.545	30.7	36.8	11.3
M-5	1.16	8.04	0.977	31.2	38.3	13.0
O-1	0.34	0.00	0.732	30.7	34.3	10.3

[1)] pre-curvature measured before testing (Figure 7)

[2)] calculated according to the shear analogy method

[3)] calculated according to JCSS [13]

[4)] determined according to EN408 [10]

3.3.3 Results

The maximum buckling load is achieved for reference series O-1, with symmetrical layup (Figure 8).

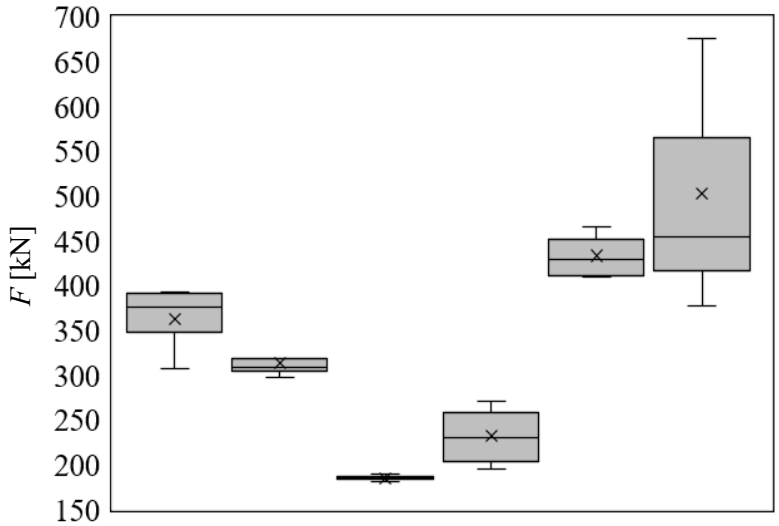

series	M-1	M-2	M-3	M-4	M-5	O-1
n [-]	4	4	4	4	4	3
mean [kN]	363	314	185	232	434	503
COV [%]	10.9	6.0	1.9	15.8	6.4	30.7

Figure 8: Buckling loads determined by experimental investigations

In comparison, the 6-layered multifunctional series M-5 with the highest bending stiffness reaches with F_{mean} = 434 kN on average 86% of the buckling load of the reference series O-1.

Figure 9 shows the comparison of the experimentally determined buckling loads with the theoretically calculated buckling loads. For this purpose, the buckling load for each series is determined using three different calculation methods: Calculation of the buckling loads according to the k_c-method (effective length method) [14], according to second-order analysis [12], and the critical buckling load p_{ki} [12].

In addition, Figure 9 shows the results for series O-1 tested with an overall eccentricity of 40 mm. For better classification of the results of the multifunctional series, the buckling load of a 3-layered reference series without channels (O-3, [20-20-20]) is additionally calculated.

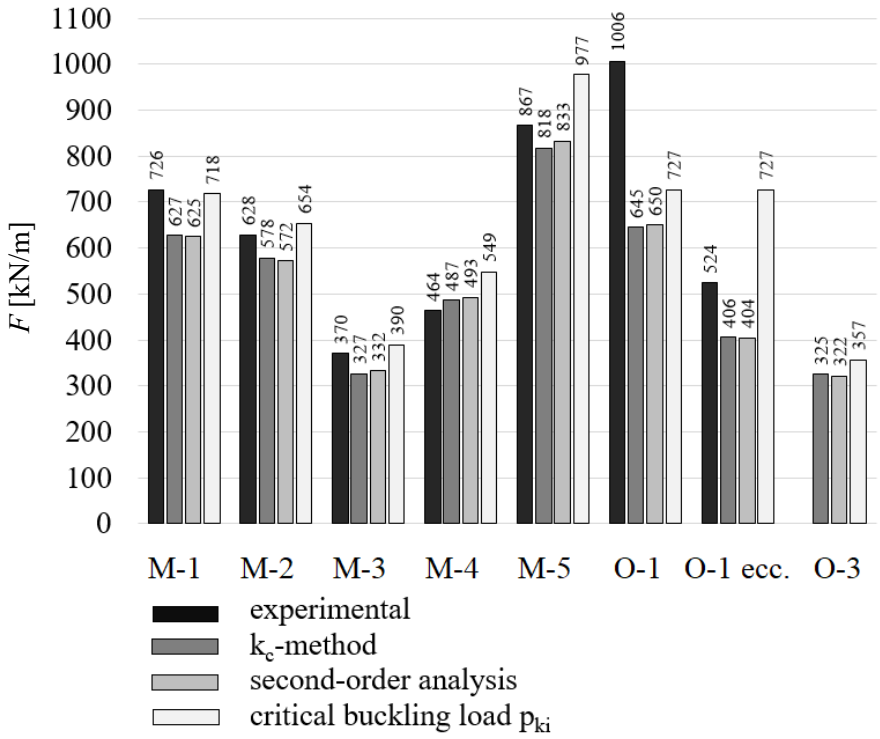

Figure 9: Comparison of the buckling loads of the experimental and theoretical investigations

The k_c-method and the second-order analysis provide good correlation to the experimentally determined buckling loads for the multifunctional series M-1 to M-5, taking into account the pre-curvature and internal eccentricity. For the five-layered reference series O-1, the maximum buckling load is underestimated by these calculation methods. The calculated critical buckling load p_{ki} provides close correlation for the multi-functional series - however, eccentricities are not taken into account for this calculation method, which makes these values less reliable.

Further evaluations of the experimental and theoretical investigation on the buckling loads such as load-deflection and stress diagrams are given in [15].

3.4 In-plane Shear Strength & Stiffness

3.4.1 Experiments

Tests were carried out according to the method proposed by Kreuzinger & Sieder [16] loading three specimens (*w/h=500mm/1250mm*) of each series under a force-to-grain-angle of 45° (Figure 10).

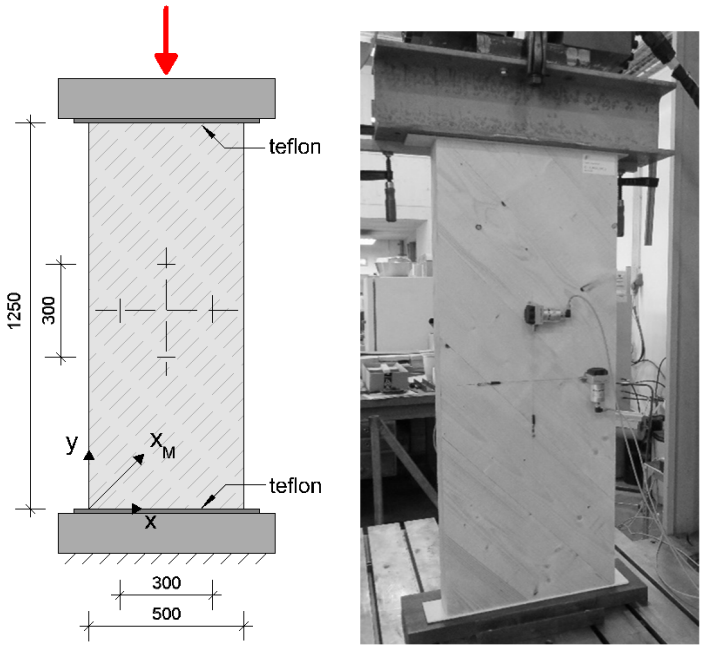

Figure 10: In-plane shear test configuration

The moisture content of each specimen was in the range of 12±2% (u_{mean} = 10.7%, COV 4.3%). The supports are made from teflon to minimize friction in x direction. The vertical (y) and horizontal (x) deflections are measured on both sides of the specimen over a length of 300 mm by means of rope displacement transducers.

3.4.2 Theoretical Investigations

In order to transfer the results to the strength and stiffness properties of multifunctional CLT, a calculation method considering the milled channels is proposed.

The in-plane failure mechanisms of the cross laminated timber elements provide information on the actual influence of the channels on the in-plane load carrying capacity (Table 4). Following the calculation method according to Brandner & Dietsch [17], the in-plane shear strength for not edge-glued CLT is calculated from the measured compression force *F* by Equation (1):

$$f_{v,net} = \frac{F}{2b \cdot d_{90}} \cdot \left(1 - \frac{E_{90}}{\frac{d_{90} \cdot E_0 + d_0 \cdot E_{90}}{d}}\right) \quad (1)$$

The fuctional layers including the channels (*40/20mm*) are not stiff enough to provide a locking-effect, break-off and will therefore not be considered in Equation (1).

This break-off results in multipart cross-sectional elements. For series M-1, for example, a three-layered not edge-glued CLT element [***20***-*20*-***20***] and a single-layered, SWP results. Consequently, the net-shear strength is calculated from the measured compression force *F* for the respective basic CLT not edge-glued element [***20***-*20*-***20***], minus the force component *F`* absorbed by the edge-glued front layer. For the single-layered SWP (front layers series M-1 and M-3), assuming a shear strength for silver fir of $f_v$ = 4.0 MPa, the force component *F`* is 83.4 kN (Equation 2).

$$F` = \tau_{xM,yM} \cdot 2 \cdot A = \frac{f_v}{\left(1 - \frac{E_{90}}{E_{yM}}\right)} \cdot 2 \cdot A \quad (2)$$

The shear moduli are calculated according to Equation (3) following the proposed method by Kreuzinger & Sieder [16] to better eliminate the influence of deformations from other stresses than shear stresses [17].

$$G_{xM,yM} = \frac{1}{\left(\frac{4}{E_y} - \frac{1}{E_{xM}} - \frac{1}{E_{yM}}\right)} \quad (3)$$

3.4.3 Results

Table 4 lists the failure mechanisms of the investigated series. For almost all specimens, a net shear failure in the basic CLT with a break-off of the functional layers can be observed in the ultimate limit state (ULS).

Table 4: In-plane failure mechanism for each specimen

Series	failure mechanism
M-1-1	net-shear failure 2nd layer [***20***-*20*-***20***]+shear failure front layer
M-1-2	net-shear failure 2nd layer [***20***-*20*-***20***]+ channels breaking off
M-1-3	net-shear failure 2nd layer [***20***-*20*-***20***]+shear failure front layer
M-2-1	net-shear failure 2nd layer [***20***-*20*-***20***]+shear failure front layer
M-2-2	net-shear failure 2nd layer [***20***-*20*-***20***]+shear failure front layer
M-2-3	net-shear failure 2nd layer [***20***-*20*-***20***]+shear failure front layer
M-3-1	net-shear failure 2nd layer [***20***-*20*-***20***]+channels breaking off
[1)]M-3-2	net-shear failure 2nd layer [***20***-*20*-***20***]
M-3-3	net-shear failure 2nd layer [***20***-*20*-***20***]+channels breaking off
M-4-1	net-shear failure 2nd and 4th layer [***20***-*20*-***20***-*20*]+channels breaking off
M-4-2	net-shear failure 2nd and 4th layer [***20***-*20*-***20***-*20*]+channels breaking off
M-4-3	net-shear failure 2nd and 4th layer [***20***-*20*-***20***-*20*]+channels breaking off
M-5-1	net-shear failure 2nd and 4th layer [***20***-*20*-***20***-*20*]+shear failure front layer
M-5-2	net-shear failure 2nd and 4th layer [***20***-*20*-***20***-*20*]+shear failure front layer
M-5-3	net-shear failure 2nd and 4th layer [***20***-*20*-***20***-*20*]+shear failure front layer
O-1-1	net-shear failure 2nd and 4th layer [***20***-*20*-***20***-*20*-***20***]
O-1-2	net-shear failure 2nd and 4th layer [***20***-*20*-***20***-*20*-***20***]
O-1-3	net-shear failure 2nd and 4th layer [***20***-*20*-***20***-*20*-***20***]

[1)] faulty gluing of the front layer - specimen is not taken into account

Table 5 gives the calculated values for the compression force of the multipart cross-sections each, the basic CLT element F_0 (using $f_{v,net}$ = 10.0 MPa according to [18]) and the individual front layer F`. The sum of these values gives the expected value of the compression force F_{th}. Comparatively the mean values of the compression forces measured during the experiment are given. Additional the percentage deviation of the expected force value F_{th} and the measured force value F_{mean} is given. The good approximation confirms the calculation method according to Brandner & Dietsch [17] when subtracting the force component absorbed by the individual front layer.

Table 5: Expected and measured compression force values

Series	M-1	M-2	M-3	M-4	M-5	O-1
[1)]F_0 [kN]	222.1	221.2	221.2	390.7	390.7	439.2
[2)]F` [kN]	83.4	79.2	83.4	/	50.0	/
[3)]F_{th} [kN]	304.6	300.4	304.6	390.7	440.7	439.2
[4)]F_{mean} [kN]	269.9	300.8	272.2	321.6	389.9	378.9
deviation [%]	12.9	0.1	11.9	21.5	13.0	15.9

[1)] force component calculated for the basic element [**20**-20-**20**] / [**20**-20-**20**-20]

[2)] force component calculated for the front-layer

[3)] results of the theoretical investigations

[4)] results of the mechanical testing

Figure 11 gives the in-plane net-shear strengths of all series.

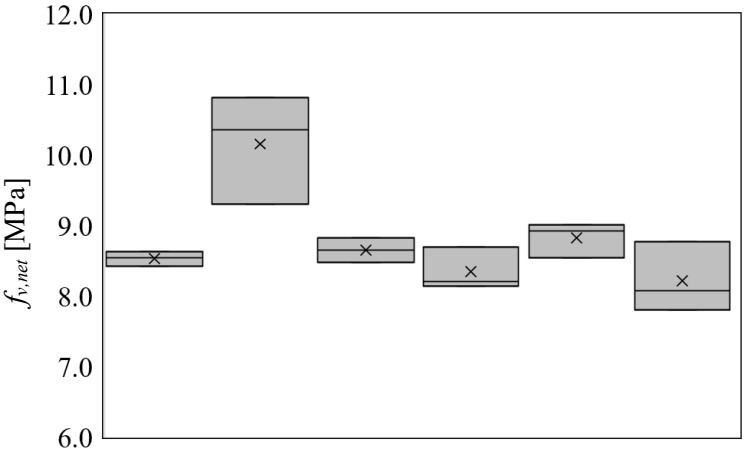

series	M-1	M-2	M-3	M-4	M-5	O-1
n [-]	3	3	2	3	3	3
mean [MPa]	8.5	10.2	8.7	8.4	8.8	8.2
COV [%]	1.2	7.6	2.8	3.6	2.8	6.0

Figure 11: In-plane net-shear strength

The positive influence of the 3-layered SWP is obvious. Due to the similar layup the shear strenght of the M-1 and M-3 series are nearly identical and on the same level as the reference CLT series O-1. Figure 12 gives the shear modulus *G* calculated according to the method of Kreuzinger & Sieder [16].

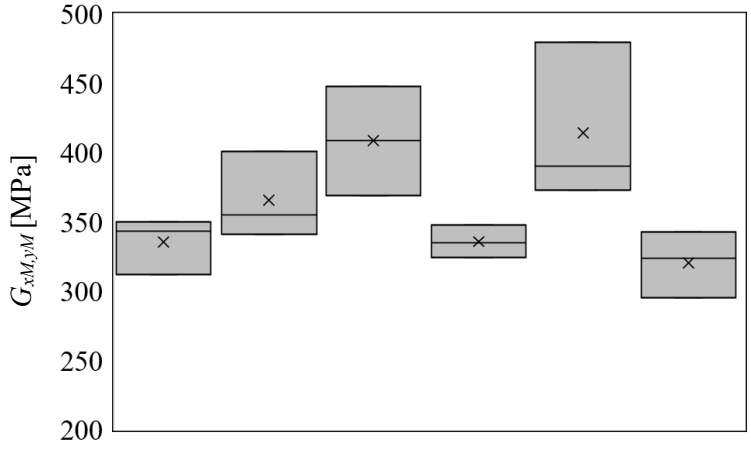

series	M-1	M-2	M-3	M-4	M-5	O-1
n [-]	3	3	2	3	3	3
mean [MPa]	335.2	365.7	408.5	335.6	414.2	320.4
COV [%]	6.0	8.5	13.7	3.5	13.8	7.5

Figure 12: In-plane shear modulus

Further evaluations and explanations of the experiments and calculation methods of the in-plane strength and stiffness properties of multifunctional CLT are given in [19].

3.5 Torsional Stiffness

3.5.1 Experiments

Square CLT specimens (*w/h=1200mm/1200mm*) are twisted in biaxial bending tests (Figure 13). The aim is to determine the torsional stiffness of the various specimens from the deformation of the elements under an external point-load.

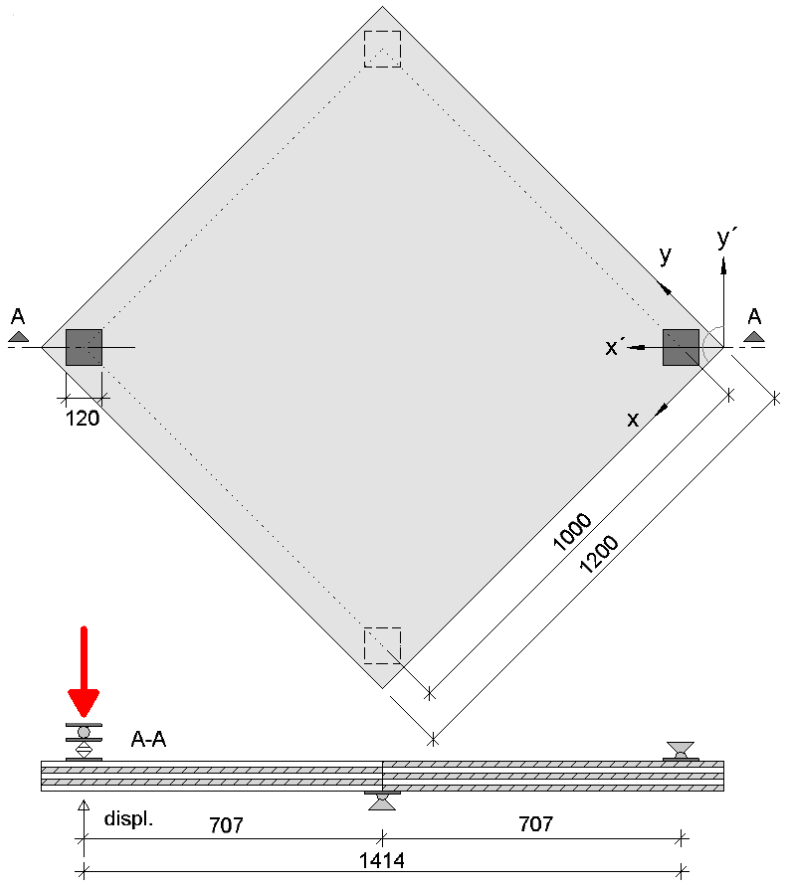

Figure 13: Test setup of the biaxial bending tests

The point-load, directed vertically downwards, is applied to the free corner of the specimens by a hydraulic cylinder. The load application point as well as the supports are realized by steel plates (*120/120/12mm*). They each are articulated and offset inwards by 100 mm from the free edges of the specimens. The deflection is measured using a rope extensometer on the opposite site of the load introduction point.

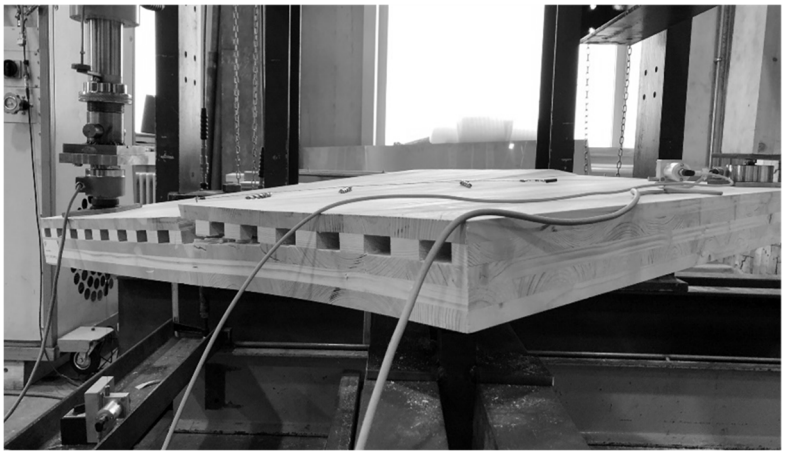

Figure 14: Biaxial bending tests on multifunctional CLT

The moisture content of the 5 series was determined to u_{mean} = 11.2 % (COV 7.6 %).

3.5.2 Theoretical Investigations

Using the method of consistent deformations (force method), the torsional stiffness of each element is calculated from the deflection *w* (Equation 4) [20].

$$B_{xy} = \frac{F \cdot dx}{2w} \tag{4}$$

A linear-elastic relationship between the applied force *F* and the deflection *w* is considered for all specimens within the range of 0.2 w_{100} to 0.5 w_{100}. Thereby w_{100} is the unit deflection of 100 mm.

3.5.3 Results

Figure 15 gives the exemplary load-deflection curves of the biaxial bending tests for one specimen of each series.

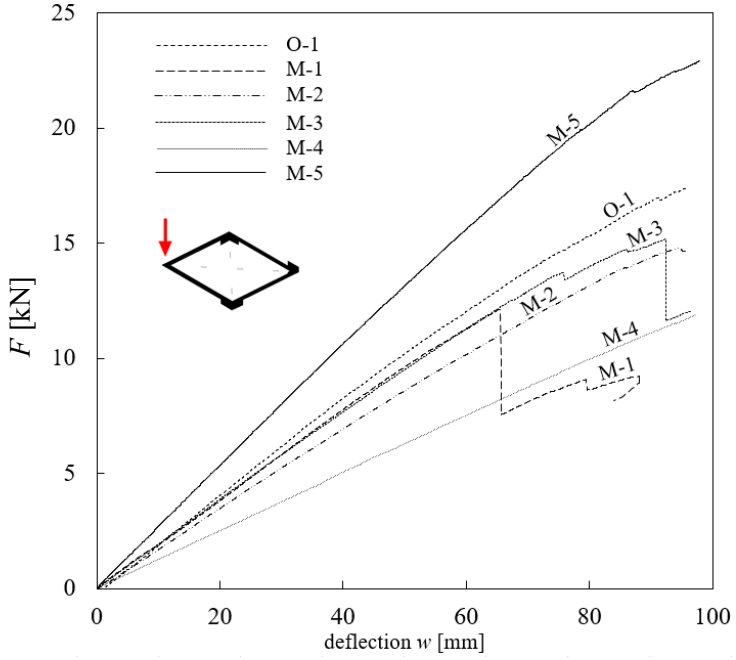

Figure 15: Load-deflection curves of the biaxial bending tests

The torsional stiffness for each series calculated by Equation 4 is given in Figure 16.

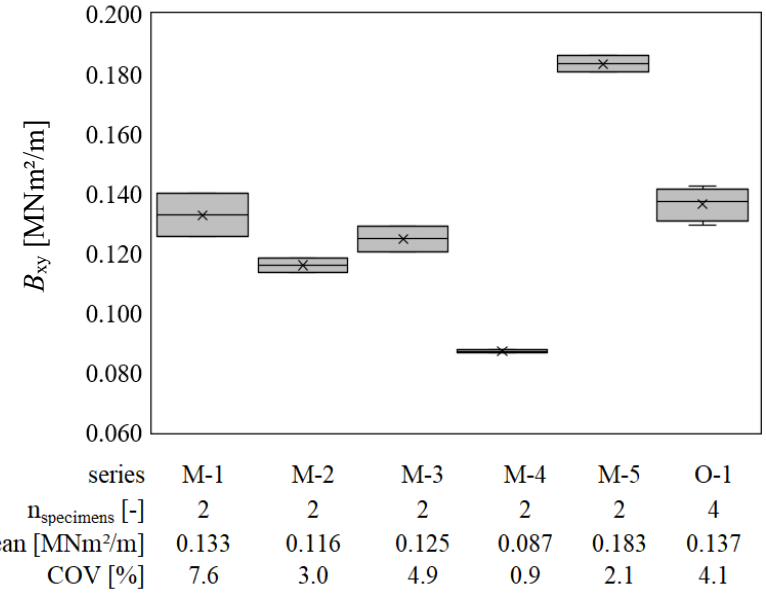

series	M-1	M-2	M-3	M-4	M-5	O-1
$n_{specimens}$ [-]	2	2	2	2	2	4
mean [MNm²/m]	0.133	0.116	0.125	0.087	0.183	0.137
COV [%]	7.6	3.0	4.9	0.9	2.1	4.1

Figure 16: Torsional stiffness values

M-5 series with the additional 6th layer has the highest torsional stiffness. The M-1, M-2 and M-3 series have a stiffness comparable to the reference CLT series O-1. The comparatively low torsional stiffness of series M-4 results form early break-off of the milled 5th layer. Thus, only 4 layers are acting under biaxial bending for the M-4 series.

4 Climatic Testing

4.1 Test Programme

The aim is to investigate the deformation behavior of the specimens during changes in the moisture content of the timber. Such moisture changes take place during the intended thermal activation via contact with the conditioned air, i.e. by diffusion. During the heating and cooling process, temperatures between 15 and 45 degrees occur in the channels of the multifunctional CLT. Table 6 lists the climatic experiments carried out.

Table 6: Climatic experiments

Experiments	processing status
Deformation Behaviour under Moisture Change	✓
Cracking of the Front Layers	✓

In Mai 2020 18 test specimens (*w/h=1000mm/500mm*) were placed in a climate chamber (Figure 17).

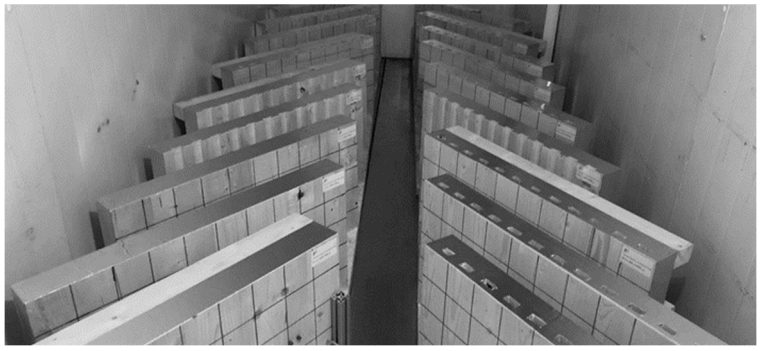

Figure 17: Moisture test specimen in the climate chamber

All surfaces of the specimens are sealed with diffusion-tight aluminum foil – except of the front layer. In addition, the channels are cut free. As a result, moisture can only diffuse into the wall elements via the front layer and the channels, as in the subsequent assembly situation. One out of three specimens per series has wooden beams screwed onto the back to prevent moisture-induced deformations. These specimens are marked in the following with a (V) after the designation. Each specimen was equipped with four permanent ram-in electrodes in depths of 70 mm, 45 mm, 25 mm and 15 mm. This allows the moisture gradient to be determined over the cross-section and its change over time.

During the six-month climatic experiment, the specimens passed through five different ambient climate phases (Figure 18).

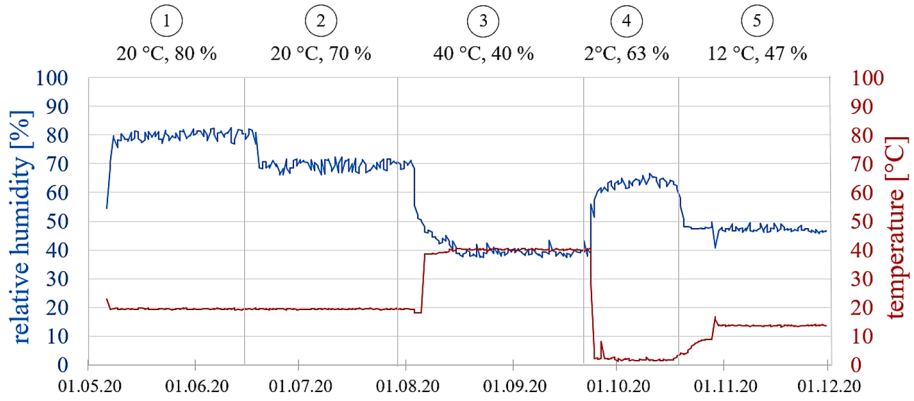

Figure 18: Phases of ambient climate in the climate chamber

Phases 1 and 2 are used to adjust the wood moisture content of the test specimens between 10 and 12 percent over the cross-section. Phase 3 simulates the thermally activated CLT elements in heating mode (40°C, 40% rel. humidity). Phase 4 is a transitory phase with the greatest possible change in humidity and temperature relative to the previous phase to bring the elements to the limits of applicability. Phase 5 simulates the cooling mode of the elements.

4.2 Deformation Behaviour under Moisture Change

4.2.1 Experiments

The overall curvature of the specimens is measured on two points of each specimen. One measuring point is located in the centre of the front layer (w_{z2}) and one measuring point is located at the upper middle of the front layer (w_{z3}). Figure 19 defines the orientation of the curvature and shows a 3-D sketch of the measuring bar.

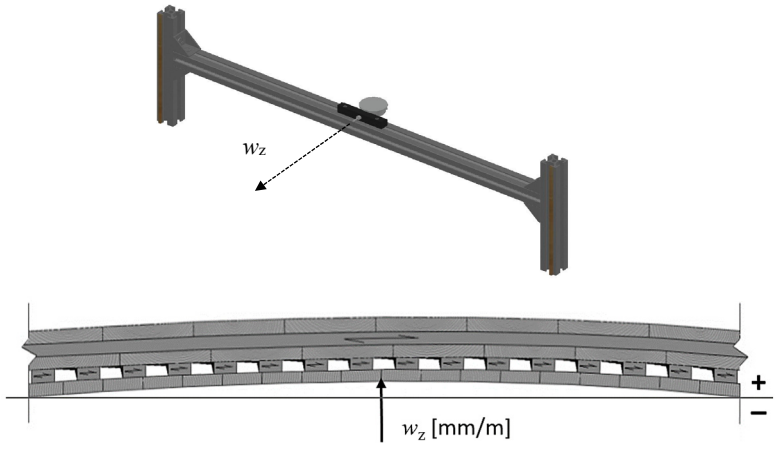

Figure 19: Test setup for determining the curvature

4.2.2 Results

Figure 20 shows the change in wood moisture content at different depths as well as the measured curvature over the different climate phases, exemplary for series M-1.

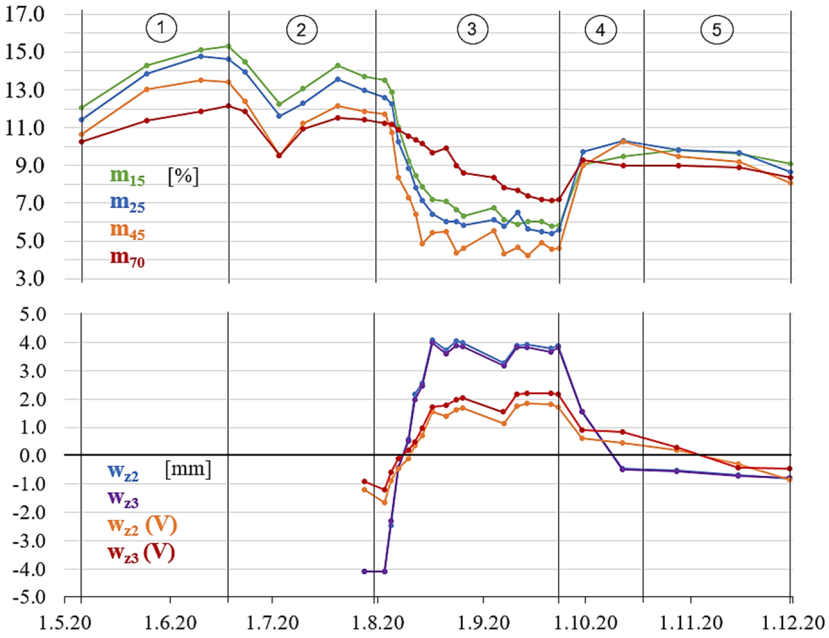

Figure 20: Moisture content and deformation of series M-1

Drying from an average of 12.2 % moisture content to about 5.8 % during phase 3 is directly accompanied by shrinkage deformation of the functional layers. This leads to a change of the overall curvature, which is expressed by an increase of more than 8 mm/m in w_{z2} and w_{z3}. The specimen of series M-1 with restrained deformation (M-1-3(V)) undergoes significantly smaller deformations, which leads to constrained stresses and consequently to increased cracking of the front layer (see chapter 4.3.2).

As a comparison to multifunctional series M-1, Figure 21 shows the moisture content and the deformation of the reference series O-1 with a symmetrical and undisturbed layup.

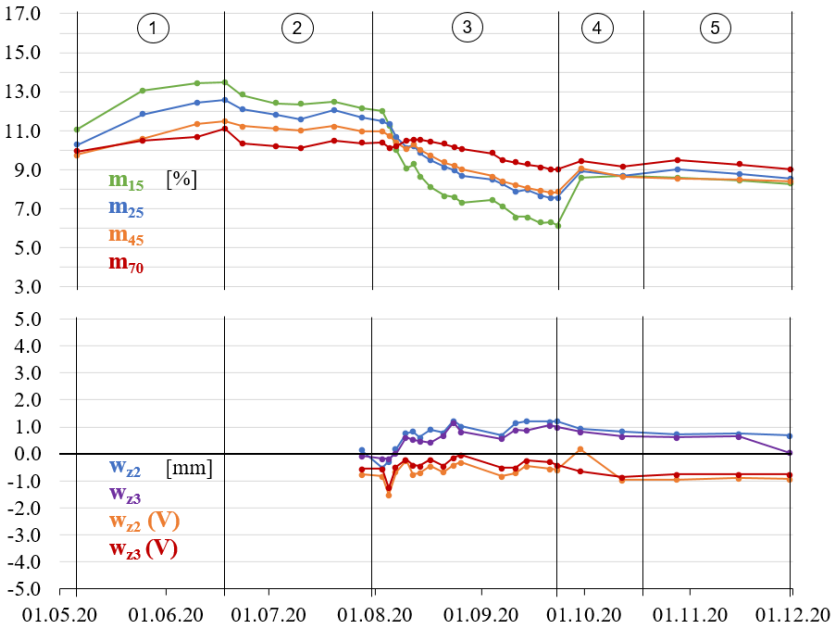

Figure 21: Moisture content and deformation of series O-1

It becomes obvious that the missing channels lead to a smaller gradient of the moisture content over the cross-section. Due to this and due to the symmetrical layup, only small deformations of approx. 2 mm/m occur – the overall curvature nearly stays flat. The reference specimen with restrained deformation (O-1-3(V)) does not show any measurable change of in curvature.

4.3 Cracking of the Front Layers

4.3.1 Experiments

Before climate phase 1 and after climate phase 3, the test specimens are examined for cracks in the front layers. The cracks are marked (red) and documented in order to draw conclusions about the robustness and airtightness of the multifunctional CLT in assembly. Figure 22 gives the exemplary crack patterns of series M-1-3(V) and O-1-2.

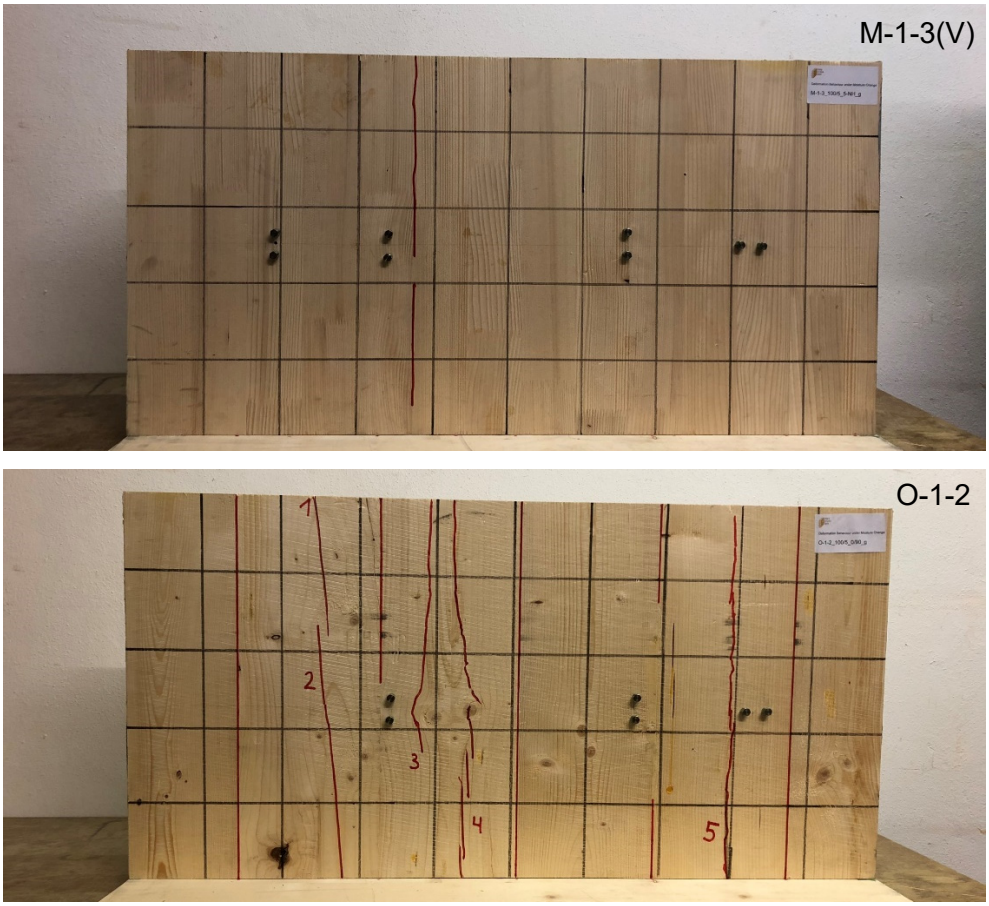

Figure 22: Exemplary crack patterns of the front layers of specimens M-1-3(V) and O-1-2 after phase 3

4.3.2 Results

Table 7 gives an overview of the visible cracks in the front layers after the heating phase (climate phase 3).

Table 7: Cracks in the front layers after climate phase 3

Series	n [-]	description of the cracks
M-1-1	0	/
M-1-2	0	/
M-1-3(V)	1	-Breaking of edge-glued lamella joint (0.15mm)
M-2-1	0	/
M-2-2	2	-Shrinkage cracks (0.15mm, 0.10mm)
M-2-3(V)	1	-Central shrinkage crack (0.20mm)
M-3-1	1	
M-3-2	3	-Breaking of edge-glued lamella joints (0.15mm, 0.55mm)
M-3-3(V)	3	-Breaking of edge-glued lamella joint (0.7mm) -Central shrinkage cracks (0.20mm, 0.40mm)
M-4-1	0	/
M-4-2	0	/
M-4-3(V)	0	/
M-5-1	0	/
M-5-2	0	/
M-5-3(V)	2	-Central shrinkage cracks (0.25mm, 0.55mm)
O-1-1	1	-Central shrinkage crack (1.00mm)
O-1-2	5	-Central shrinkage cracks (0.40-1.40mm)
O-1-3 (V)	7	-Central shrinkage cracks (0.50-1.60mm)

Further results of the climatic testing as well as numerical FEM simulations on moisture transport in multifunctional CLT during cyclic heating and cooling operations are given in [21].

5 Conclusions

Multifunctional cross laminated timber takes massive timber construction to a new level of usability and serviceability. Compared to conventional CLT, whose advantages are mainly limited to its mechanical properties, multifunctional CLT opens up a multitude of different application areas and opportunities - such as the integration of building services - or room conditioning through thermal activation.

The findings from this research project have already proven that neither the asymmetric layup nor the channels significantly reduce the load-bearing capacity of the multifunctional massive timber elements. So far the main outcomes of this research are:

- The reduction of the cross-sectional area through the channels does not necessarily have a significant influence on the compression strength and stiffness of the elements
- With regard to the determination of the in-plane shear strength and stiffness, the channels cause a break-off of the functional layers and as a result a net shear failure of the remaining cross-section. However, due to the high quality of the edge-glued front layers, the shear stiffness of the full multifunctional cross-sections is at the same or higher level than that of conventional CLT.
- The buckling loads of the multifunctional series are lower than those of the reference series, i.a. because the channels lead to a change in the centre of gravity of the elements and thus to an eccentricity. With an average initial buckling load of 0.61 MN/m, the multifunctional series prove resistant enough to be used as load-bearing walls. The buckling load is many times higher than that of timber frame constructions of a comparable thickness.
- The extensive climatic testing demonstrates clearly that the quality of the front layer is of decisive importance for the deformation behavior and crack pattern under thermal stress. It is therefore advisable to use high-quality 1-layered better 3-layered solid wood panels for the outer layer.

In the further progress of this research project, the contribution of the multifunctional layers to the fire resistance as well as the behavior in case of cavity fires is investigated. In addition, a catalogue of applicable connection techniques for multifunctional CLT panels will be developed.

The potential of multifunctional CLT is obvious. The elimination of visible radiators creates additional architectural value and increases the level of comfort. Integrating the production of a large number of specimens into the standard CLT production process has demonstrated that manufacture of multifunctional wall elements can be feasible and even economical in the near future.

Acknowledgement

The project is funded by Fachagentur Nachwachsende Rohstoffe e. V. (FNR) of the German Federal Ministry of Food and Agriculture (BMEL) in the frame of the ForestValue project InnoCrossLam. The production of the multifunctional CLT was done by Lignotrend Produktions GmbH. The basic CLT elements were provided by Pfeifer Timber.

References

[1] Mindrup K., Winter S.: Thermal activation of solid timber elements for indoor climate control. Conference Paper, WCTE. Seoul, 2018.

[2] Mindrup K.: Room climate conditioning using thermally activated solid timber elements. Concept development, performance analysis and derivation of design tool. Dissertation. Technical University of Munich. Munich, 2020.

[3] ETA-20/0023, European Technical Assessment, Pfeifer CLT Brettsperrholz, Austrian Institute of Construction Engineering. Vienna, 2020.

[4] Z-9.1-765, Allgemeine bauaufsichtliche Zulassung, 1K-PUR-Klebstoffe "Loctite HB S049 bis HB S709 Purebond" für die Verklebung tragender Holzbauteile. DIBt – Deutsches Institut für Bautechnik. Berlin, 2016

[5] DIN EN 301 - 2018-01 Klebstoffe, Phenoplaste und Aminoplaste, für tragende Holzbauteile - Klassifizierung und Leistungsanforderungen; PUR adhesive. DIN – Deutsches Institut für Normung. Berlin, 2018.

[6] Z-9.1-691, Allgemeine bauaufsichtliche Zulassung, 1K-PUR-Klebstoff "Jowapur 686.30" für die Verklebung tragender Holzbauteile. DIBt – Deutsches Institut für Bautechnik, Berlin, 2017.

[7] EN 12775:2001, Solid wood panels - Classification and terminology. CEN – Comité Européen de Normalisation. Brussels, 2001.

[8] EN 13986:2004+A1:2015, Wood-based panels for use in construction - Characteristics, evaluation of conformity and marking, CEN – Comité Européen de Normalisation. Brussels, 2015.

[9] EN 13353:2008+A1:2011, Solid wood panels (SWP) – Requirements. CEN – Comité Européen de Normalisation. Brussels, 2011.

[10] EN 408:2012: Timber structures – Structural timber and glued laminated timber – Determination of some physical and mechanical properties. CEN – Comité Européen de Normalisation, Brussels, 2012.

[11] Kreuzinger H.: Verbundkonstruktionen aus nachgiebig miteinander verbundenen Querschnitts-teilen. Tagungsband. Ingenieur-holzbau Karlsruher Tage 2000. Bruderverlag, Karlsruhe, 2000.

[12] DIN EN 1995-1-1/NA:2013-08, National Annex - Nationally determined parameters - Eurocode 5: Design of timber structures - Part 1-1: General - Common rules and rules for buildings. DIN – Deutsches Institut für Normung. Berlin, 2013.

[13] JCSS probabilistic model code Part 3: resistance models 3.5 properties of timber. Joint Committee on Structural Safety, 2006.

[14] EN 1995-1-1:2010, Eurocode 5: Design of timber structures - Part 1-1: General - Common rules and rules for buildings, Chapter 6.3. CEN – Comité Européen de Normalisation. Brussels, 2010.

[15] Gabel S.: Experimentelle Untersuchung des Knickverhaltens multifunktionaler Brettsperrholz-Wandelemente. Master´s Thesis. Technical University of Munich. Munich, 2020.

[16] Kreuzinger H., Sieder M.: Einfaches Prüfverfahren zur Bewertung der Schubfestigkeit von Kreuzlagenholz/Brettsperrholz. Bautechnik, 90(5): 314-316, Berlin, 2013.

[17] Brandner R., Dietsch P., Dröscher J., Schulte-Wrede M., Kreuzinger H., Sieder M.: Cross laminated timber (CLT) diaphragms under shear: Test configuration, properties and design. Construction and Building Materials, 147:312-327, 2017.

[18] Brandner R., Bogensperger T., Schickhofer G.: In plane Shear Strength of Cross Laminated Timber (CLT): Test Configuration, Quantification and influencing Parameters. CIB-W18/46-12-2, Vancouver, 2013.

[19] Niebauer S.: Experimentelle Untersuchung der Scheibenschubfestigkeit und -steifigkeit von thermisch aktivierbarem Brettsperrholz. Master´s Thesis. Technical University of Munich. Munich, 2020.

[20] Mestek P., Winter S., Kreuzinger H.: Brettstapeln, Brettsperrholz und Verbundkonstruktionen. Teilprojekt 15 des HTO- Verbundforschungs-vorhabens "Holzbau der Zukunft". Technical University of Munich. Munich, 2008.

[21] Fochler D.: Verformungsverhalten von thermisch aktiviertem Brettsperrholz unter nutzungsbedingten Feuchtigkeitsänderungen. Master´s Thesis. Technical University of Munich. Munich, 2021.